TFEC-2018-22038

AN APPLICATION OF THE MONTE CARLO RAY-TRACE METHOD WITH BIDIRECTIONAL REFLECTION

J. Robert Mahan[1]*, N. Q. Vinh[1], and Kory J. Priestley[2]

[1]Virginia Polytechnic Institute and State University, Blacksburg, VA 24061, USA
[2]NASA Langley Research Center, Hampton, Virginia 23682, USA

ABSTRACT

Surface bidirectionality must be considered when high accuracy is required of a radiative exchange model. Presented is an adaptation of the Monte Carlo ray-trace (MCRT) method for treating bidirectional reflections. Each incident ray is split into a family of reflected rays whose power and direction are determined based on a new four-component model for the bidirectional reflectance distribution function (BRDF) of Z302, an optical coating widely used in aerospace applications. The model is based on BRDF data available in the literature. We validate the model by using it to simulate the performance of a device for measuring the BRDF of a Z302 sample. We find that the difference between the original BRDF, upon which the bidirectional reflectivity model is based, and the BRDF recovered from the simulation depends on the physical resolution of the detector geometry and the number of rays traced.

KEY WORDS: Radiation Heat Transfer, Monte Carlo Ray Trace Method, Bidirectional Reflection

1. INTRODUCTION

The directional distribution of reflected radiation is known to be strongly influenced by the topography, chemical properties, and degree of contamination of the surface. Therefore, it is unlikely that a wavelength-dependent, bidirectional reflectivity model based entirely on theory could accurately represent the optical behavior of most surfaces of practical engineering interest. In cases where high accuracy is required, a successful surface optical model must be at least semi-empirical if not based entirely on measurements.

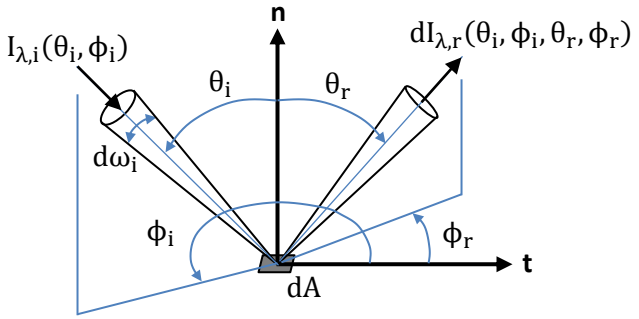

Fig. 1 Beams of monochromatic light incident to and reflected from an area element dA.

The monochromatic bidirectional reflectivity is defined[1]

$$\rho_\lambda''(\lambda, \theta_i, \phi_i, \theta_r, \phi_r) \equiv \frac{dI_{\lambda,r}(\lambda,\theta_i,\phi_i,\theta_r,\phi_r)}{I_{\lambda,i}(\lambda,\theta_i,\phi_i)\cos\theta_i d\omega_i}, \quad (1)$$

where I_λ is the monochromatic intensity, or radiance ($W/m^2 \cdot sr \cdot \mu m$), of the light in spectral interval $\Delta\lambda$ surrounding wavelength λ, and the subscripts *i* and *r* are associated with the incident and reflected beams, respectively. The geometry is illustrated in Fig. 1. The monochromatic bidirectional reflectivity is often

*Corresponding Author: jrmahan@vt.edu

referred to as the bidirectional reflectance distribution function, or BRDF. The BRDF is important because it includes all information needed to compute the other surface optical properties.

The effort reported in this contribution is based on the conventional Monte-Carlo ray-trace (MCRT) method.[1] While many previous contributions have reported efforts to model radiant interchange in enclosures whose walls exhibit bidirectional behavior, relatively few are particularly relevant to the effort reported here. Ono[2] used a Monte Carlo approach to evaluate the nested integrals that arise from the analytical formulation of radiant exchange within a diffuse-specular enclosure, and Sapritsky and Prokhorov[3] report use of a Monte Carlo algorithm to compute the effective emissivities of diffuse-specular cavities for use in radiometry. Ohwada[4] assumed a relatively simple single-parameter model for non-Lambertian surface behavior and used numerical integration rather than the MCRT method to evaluate the nested integrals that arise in the formulation. An influential 1998 article by Prokhorov[5] presents original MCRT algorithms and related software for predicting the absorption characteristics of cavity radiometers. Finally, a recent article by Prokhorov and Prokhorova[6] provide the impetus for the current contribution. In the cited article the authors present a very useful dataset, reproduced in Fig. 2, representing the measured bidirectional reflectivity of a widely used optical coating, Z302.[7] They derive a three-component BRDF model based on their original data and then use it in an MCRT model to predict the effective emissivity of a blackbody cavity intended for use in radiometric calibration.

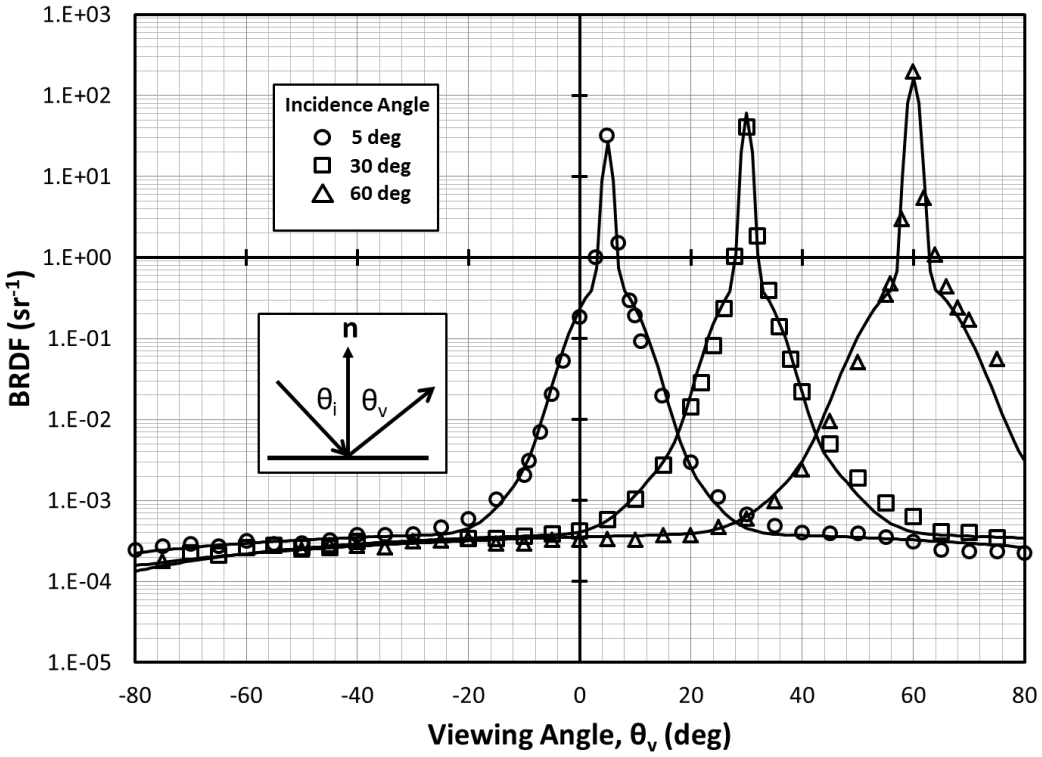

Fig. 2 Empirical model fit (curves) to Prokhorov and Prokhorova[6] data (symbols).

2. DERIVATION OF A BRDF MODEL FOR Z302

Aeroglaze® Z302 (Lord)[7] is a polyurethane-based paint whose absorptivity typically exceeds 90 percent in the visible part of the spectrum, depending on the wavelength and coating thickness. It is unique in that the reflected component of radiation is mostly specular. Its special properties make it the coating of choice for many aerospace and optical applications where a surface must be an exceptionally efficient absorber, but where diffuse reflection is undesirable. A typical application is the interior surface of a blackbody cavity used as a calibration target. In this case the cavity geometry would be such that several specular reflections would occur before an incident ray could escape. In this case any diffuse component of reflectivity present would diminish the effectiveness of the design because it would allow some power to escape the cavity with each reflection. Such diffuse "leaks" can be significant when the effective emissivity of the cavity must be unity to better than three nines.

Prokhorov and Prokhorova[6] describe a three-component semi-empirical model based on their measurements, represented by the symbols in Fig. 2, of the BRDF of Z302 at a wavelength of λ = 10.6 μm. We have used the same data to derive a purely empirical four-component model, represented by the curves in the figure. Both the Prokhorov and Prokhorova model and our model appear to be in excellent agreement with the measurements. Our goal is to demonstrate that we can begin with a reasonably realistic BRDF model and eventually recover the original data upon which it is based by running a simulated BRDF measurement experiment. Therefore, we have not performed a formal goodness-of-fit analysis between the data and BRDF our model. Our four-component has the form

$$\text{BRDF} = \rho_1'' + \rho_2'' + \rho_3'' + \rho_4'' \,, \tag{2}$$

where

$$\rho_n'' = A_n \frac{1}{\sqrt{2\pi}\sigma_n} e^{-(\theta_v - \theta_i)^2/2\sigma_n^2} + O_n \,, \; n = 1, 2, 3, 4. \tag{3}$$

In Eq. (3), θ_i and θ_v are the incidence and viewing angles shown in the inset in Fig. 2, and A_n, σ_n and O_n are empirical curve-fitting parameters. The form of Eq. (3) is recognizable as the normal distribution function multiplied by a scaling factor A_n and shifted in amplitude by an offset O_n. In practice the additive offsets for the four values of n are gathered into a single constant. The fit illustrated in Fig. 2 was obtained by defining the standard deviation

$$\sigma_n = \frac{1}{\sqrt{2\pi} b_n \theta_i} \tag{4}$$

and the multiplicative constant

$$A_n = \frac{B_n}{b_n \theta_i} \,, \tag{5}$$

where the coefficients B_n and b_n and the offset are given in Table 1.

Table 1 Fitting parameter values for the model shown in Fig. 2.

θ_i	b_1	B_1	Offset	b_2	B_2	b_3	B_3	b_4	B_4
5	0.000250	0.005	0.0046	0.0100	0.01	0.0200	0.5	0.12	32.1
30	0.000040	0.005	0.0046	0.0015	0.01	0.0035	0.5	0.02	40.8
60	0.000015	0.005	0.0046	0.0016	0.01	0.0015	0.5	0.01	195

We see that the coefficients B_1, B_2, B_3 and the offset are constants, while the coefficients b_1, b_2, b_3, b_4, and B_4 are functions of the incidence angle, θ_i. The variations of these latter parameters with incidence angle are illustrated in Figs. 3 and 4, which include the corresponding fitting equations. The Prokhorov and Prokhorova data were lifted from Fig. 3 in Ref. 6 using an optical scanner and picking off values from the indicated cursor position. The accuracy thus obtained is deemed to be in keeping with the goals of the effort as stated above.

The similarity of form among the fits for b_n suggests that they are governed by a common physical principle. Note that the values for b_n are unbounded at $\theta_i = 0$. Therefore, since values of θ_i approaching zero may occur in a practical ray-trace, it is necessary to artificially limit these parameters below a certain threshold value of θ_i. In the case at hand we use the rule that if $\theta_i < 1$ deg, $b_n = b_n(1 \text{ deg})$. The overall error introduced by this rule is negligible because of the relatively small number of incidences of $\theta_i < 1$ deg, but especially because the value of the exponential in Eq. (3) rapidly approaches 1.0 as θ_i decreases below 1 deg. The fit for the variation of the coefficient B_4 with incidence angle is given in Figure 4.6. The choice of a log-linear fitting function is justified because only three observations are available. A more elegant fitting function might produce a better fit but, using only three data points, such a fit would place too much weight on a single observation. Once again, this level of curve fitting accuracy is consistent with the goal of the effort, which is to derive a realistic BRDF model and then use it in the MCRT environment to recover the original data. The degree of success in accomplishing this goal, reported elsewhere in this contribution, tends to justify the decision. We do not claim that our four-component model represents the true bidirectional reflectivity of

Z302. However, it is probably true that our model would fall within the sample-to-sample variation observed in commercial applications, when variabilities in coating thickness and substrate morphology and preparation are taken into account.

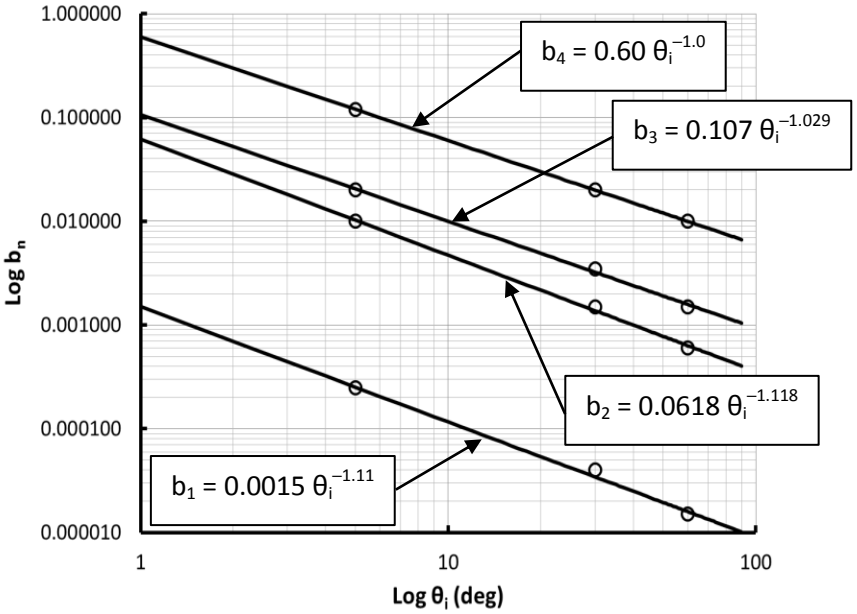

Fig. 3 Models for b_n coefficients (symbols are values from Table 1).

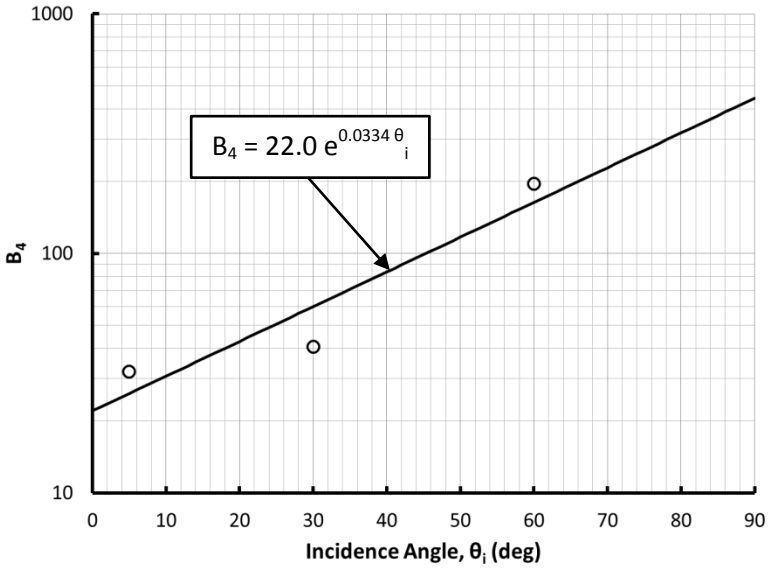

Fig. 4 Model for B_4 coefficient (symbols are values from Table 1).

We now have an analytical tool for characterizing the bidirectional reflectivity, or BRDF, of Z302 near 10.6 μm. However, this model describes the surface optical behavior only for viewing angles in the plane of incidence. How do we predict the reflectivity at viewing angles out of the plane of incidence? Following Prokhorov and Prokhorova, we assume axisymmetry in the directional reflection pattern about the axis running from the point of reflection in the direction of the viewing zenith angle, θ_v. Subject to this reasonable assumption, the model represented by Eqs. (2) and (3) is valid for all viewing angles if $\theta_v - \theta_i$ in Eq. (3) is replaced by γ, where

$$\gamma = (180.0/\pi)\ \cos^{-1}[\mathbf{v}_r \cdot \mathbf{v}_v]\ \text{(deg)}. \tag{6}$$

In Eq. (6)

$$\mathbf{v}_r = (x_r - x_1)\,\mathbf{i} + (y_r - y_1)\,\mathbf{j} + (z_r - z_1)\,\mathbf{k} \tag{7}$$

and

$$\mathbf{v}_v = (x_v - x_1)\,\mathbf{i} + (y_v - y_1)\,\mathbf{j} + (z_v - z_1)\,\mathbf{k}\,, \tag{8}$$

where (x_1, y_1, z_1) is the point on the surface where the ray is incident, (x_r, y_r, z_r) is a point on the surface of a unit hemisphere intersected by a diffusely reflected ray, and (x_v, y_v, z_v) is the point on the unit hemisphere intersected by a ray at the viewing angle θ_v, as illustrated in Fig. 5.

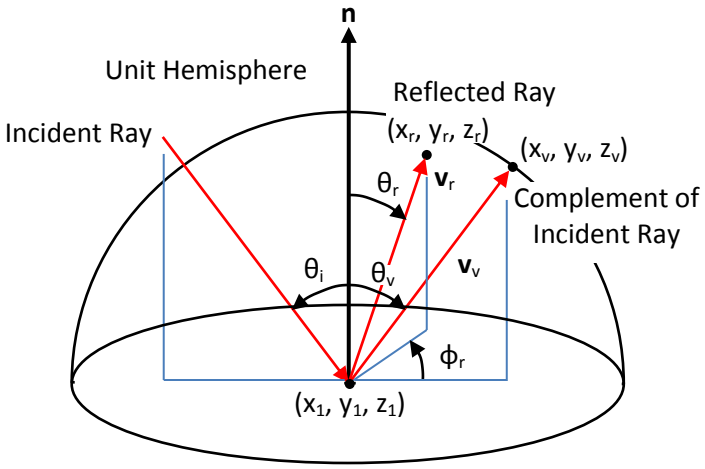

Fig. 5 Geometry defining $\mathbf{v}_r$ and $\mathbf{v}_v$ in Eqs. (9) through (11). (θ_i and θ_v are both in the plane of incidence and the points (x_v, y_v, z_v) and (x_r, y_r, z_r) both lie in the surface of the unit hemisphere.)

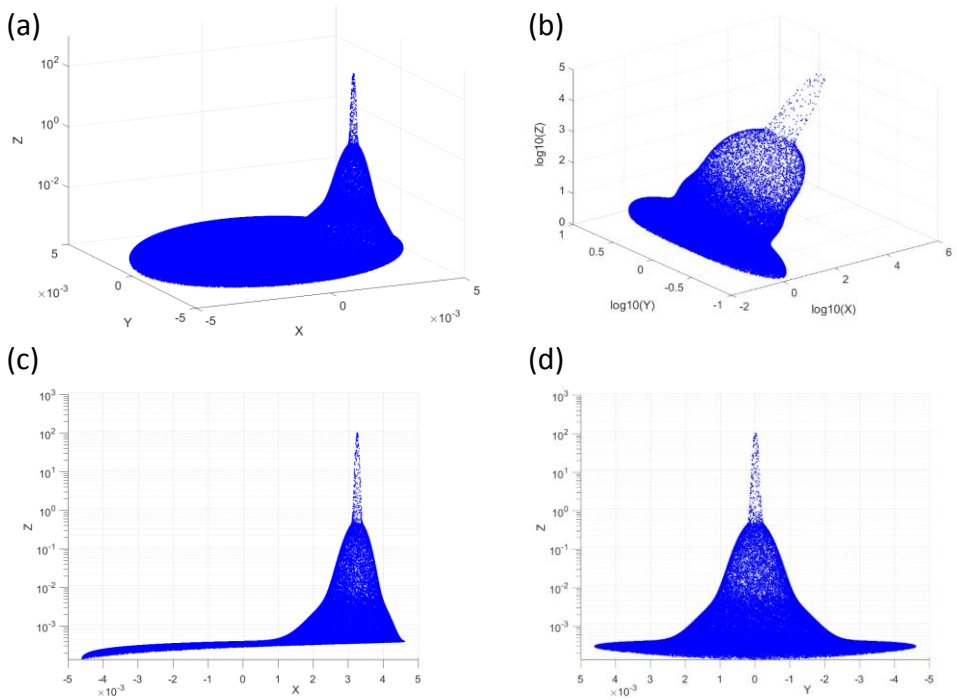

Fig. 6 Four views of the BRDF pattern produced by 100,000 rays incident at 45 deg: (a) isometric view, (b) logarithmic view (c) view normal to x-axis, (d) view normal to y-axis.

Figure 6 represents four views of the same the BRDF distribution corresponding to 100,000 rays created by the splitting of a single ray incident at (x, y, z) = (0, 0, 0) at an angle of 45 deg according to the four-component bidirectional reflectivity model. The illuminated sample lies in the x,y-plane. All rays carry the same power.

The various coefficients comprising the model presented here are of course particular to Z302 at 10.6 μm applied to the thickness of the coating studied by Prokhorov and Prokhorova. In general, the values of the model coefficients can be expected to vary with both wavelength and coating thickness. Prokhorov and Prokhorova report that the wavelength dependence of Z302 is rather weak in the interval surrounding 10.6 μm, and they suggest that modeling parameters determined at this wavelength can probably be used across the 8-to-12-μm range with acceptable error. It is difficult to overstate the need for conducting a serious experimental campaign aimed at characterizing the optical behavior of the actual surface coatings to be used in an application requiring a high level of accuracy.

3. APPLICATION OF BIDIRECTIONAL MODELS IN THE MCRT ENVIRONMENT

Once the BRDF model has been created, the directional absorptivity may be determined as

$$\alpha'(\theta_i) = 1 - \rho'(\theta_i)\,, \tag{9}$$

where

$$\rho'(\theta_i) = \mathrm{DHR} = \int_0^{2\pi}\int_0^{\pi/2} \rho''(\theta_i, \theta_r, \phi_r)\cos\theta_r \sin\theta_r d\theta_r d\phi_r \tag{10}$$

is the directional-hemispherical reflectivity (DHR). The integration implied by Eq. (10) is approximated in the MCRT environment as

$$\rho'(\theta_i) = (2\pi/M)\sum_M \rho''(\theta_i, \theta_r, \phi_r)\ , \tag{11}$$

where the sum is over the number M of reflected rays and $2\pi/M$ is the mean solid angle into which each ray is reflected. The careful reader might notice that the factor $\cos\theta_r$ in Eq. (10) does not appear explicitly in Eq. (11) but rather is invoked implicitly in the definition of θ_r, given in Eq. (14), during summation.

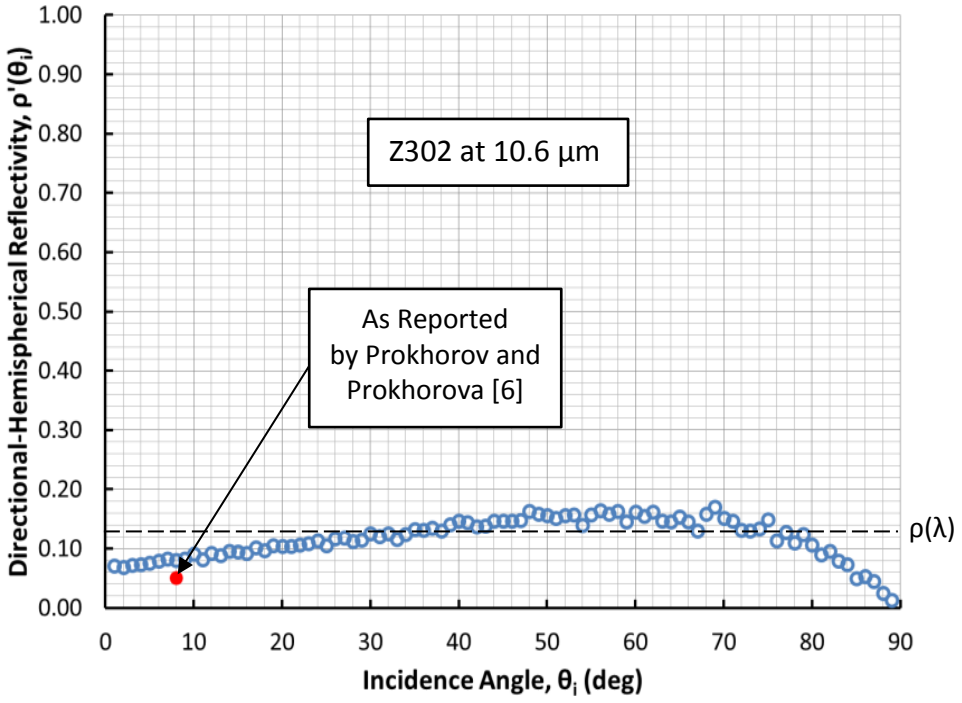

Fig. 7 The variation of the directional-hemispherical reflectivity of Z302 at λ = 10.6 μm computed using Eq. (11) with the four-component model for $\rho''(\theta_i, \theta_r, \phi_r)$.

MCRT-based results for the variation with incidence angle of the directional-hemispherical reflectivity, Eq. (10), and the directional absorptivity, Eq. (9), are plotted in Figs. 7 and 8, respectively. Prokhorov and Prokhorova report a value of about 0.051 (read from Fig. 4 in Ref. 3) for the directional-hemispherical reflectivity of their sample for an incidence angle of 8 deg. This value is also plotted in Fig. 7, which shows the values of directional-hemispherical reflectivity obtained using the four-component model for

$\rho''(\theta_i, \theta_r, \phi_r)$. The agreement between the directly measured value at an incidence angle of 8 deg and the value obtained using the model—within three percent—is remarkably good considering that the two methods for determining $\rho'(\theta_i)$ are based on two different independent experiments, with data from one of them interpreted using a complex model.

The horizontal dashed line in Fig. 7 is drawn at the level of the bi-hemispherical reflectivity $\rho(\lambda)$ as estimated in the MCRT environment using

$$\rho(\Delta\lambda) \equiv \frac{\int_{2\pi_r} \Phi_r(\Delta\lambda,\theta_r,\phi_r)\mathrm{d}\Omega_r}{\int_{2\pi_i} \Phi_i(\Delta\lambda,\theta_i,\phi_i)\mathrm{d}\Omega_i} \approx \frac{\sum_n P_{r,n}(\Delta\lambda,\theta_r,\phi_r)/(2\pi R^2)}{\pi I(\Delta\lambda)} \ , \tag{12}$$

where $\Phi_r(\Delta\lambda, \theta_r, \phi_r)$ is the reflected flux (W/m^2) in direction (θ_r, ϕ_r), and $\Phi_i(\Delta\lambda, \theta_i, \phi_i)$ is the incident flux from direction (θ_i, ϕ_i). The summing index n in Eq. (12) refers to the number of detector positions required to effectively "cover" the hemispherical surface in which the detector is displaced. The accuracy of the estimate increases with the number of positions $n = 2\pi R^2/A_D$. In practice, $\rho(\Delta\lambda)$ is usually measured separately using an integrating sphere. Finally, the power absorbed in the surface element containing the point of incidence is

$$P_a = P_i\, \alpha(\theta_i) \ . \tag{13}$$

Two MCRT continuations are available:

(1) Compare the value of $\alpha(\theta_i)$ with a random number R_α. If $\alpha(\theta_i) > R_\alpha$, the ray is absorbed, in which case a new ray is launched. Otherwise, the ray is reflected and continues at full strength, with the direction of reflection determined by a statistical process, described below, based on the bidirectional reflectivity model.

(2) Reduce the power carried by the ray by an amount P_a and then compare its remaining power $P_r = P_i - P_a$ with a threshold value. If, for example, $P_r < P_o \times 10^{-6}$, where P_o is the power carried by the ray before its first reflection, the ray is terminated and a new ray is launched. Otherwise, the ray continues onward at its reduced strength.

The two schemes listed above both lead to the same overall result if a sufficiently large number of rays are traced. Before either of these two schemes can be implemented, we must first use Eqs. (9) and (10) to compute the directional absorptivity $\alpha(\theta_i)$. This requires that a ray trace be performed in which a large number M of reflections are presumed to occur from the point of incidence. This step is necessary even if it is subsequently determined that no reflection occurs.

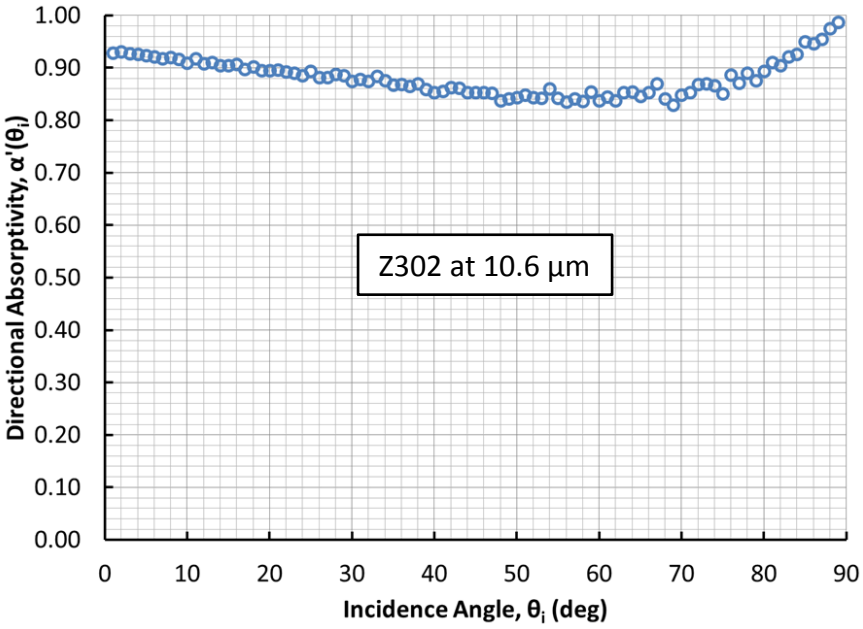

Fig. 8 The variation of the directional absorptivity of Z302 at $\lambda = 10.6$ μm computed using Eqs. (9) and (13) with the four-component model for $\rho''(\theta_i, \theta_r, \phi_r)$.

Referring to Fig. 5, a random direction $\mathbf{v}_r$ is assigned to each of the M reflections in the usual manner for diffuse reflections. That is,

$$\theta_r = \sin^{-1}[\sqrt{R_\theta}] \text{ and } \phi_r = 2\pi R_\phi \,, \tag{14}$$

where R_θ and R_ϕ are random numbers whose values are uniformly distributed between zero and unity. Then $x_r = \sin\theta_r\cos\phi_r$, $y_r = \sin\theta_r\sin\phi_r$, and $z_r = \cos\theta_r$, followed by application of Eq. (7). The direction $\mathbf{v}_v$ is obtained using Eq. (8) with $x_v = \sin\theta_v$, $y_v = 0$ (since $\theta_v = \theta_i$ and $\phi_v = 0$), and $z_v = \cos\theta_v$. The angle γ is then computed using Eq. (6), after which Eqs. (2) and (3) are used to compute the bidirectional reflectivity, $\rho''(\theta_i, \theta_r, \phi_r)$. The directional-hemispherical reflectivity $\rho'(\theta_i)$ may now be computed using Eq. (11).

Figure 7 reveals that the directional-hemispherical reflectivity approaches zero as the angle of incidence approaches 90 deg. This seems to contradict the trend for the BRDF shown in Fig. 2, which suggests an increase in directional-hemispherical reflectivity with incidence angle. However, this intuitive reasoning does not take into account the effect of the weight factor $\cos\theta_r$ in Eq. (10) and the corresponding directional reflection distribution inherent in Eq. (14). Because the peak in BRDF always occurs at $\theta_r = \theta_v = \theta_i$, this factor dominates the trend at large incidence angles.

4. DEMONSTRATION OF THE METHOD

The method may be briefly but effectively demonstrated by simulating the measurement of the BRDF of a coupon coated with Z302 using the apparatus illustrated schematically in Fig. 9. In the simulation, we illuminate the Z302-coated coupon with a collimated 2.0-mm diameter circular beam of power P_s incident at 45-deg. The beam is composed of a bundle of N = 1000 randomly spaced parallel rays, each carrying a power of P_i = 10.0 mW. Upon incidence to the Z302-coated coupon, each ray is split into M = 100,000 raylets which are reflected into the hemispherical space above their point of incidence. In the simulation we set the distance R in Fig. 4.3 to 100 mm to ensure that the detector lies in the far field of the intersection of the beam with the coupon.

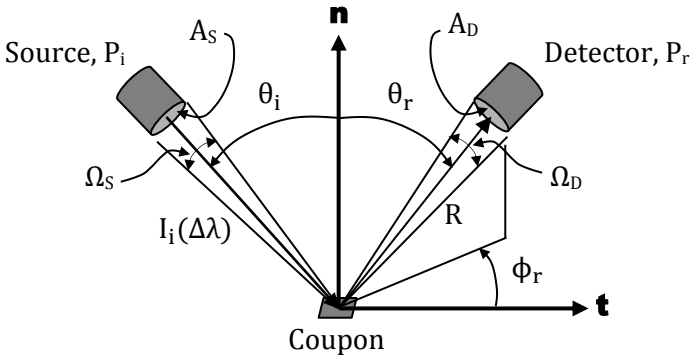

Fig. 9 Schematic representation of an apparatus for measuring the BRDF of a coupon.

Figure 10 shows the simulated power measured by the detector as it is displaced at constant azimuth angle $\phi_d = 0$ over a range of zenith angles $15 \le \theta_d \le 75$ deg. The power measured by the detector depends on the number of rays incident to it, which in turn depends on the solid angle subtended by the detector at the center of the illuminated spot on the coupon. Reference to Fig. 7 suggests that about 90 percent of the incident power, about 9 W in this case, is expected to be absorbed, while the remaining 1 W or so is reflected into the hemispherical space above the coupon.

It now remains to convert the power distribution into BRDF. The power incident to the detector for a given incidence angle θ_i and corresponding solid angle Ω_i due to N incident rays and M reflected rays per incident ray is

$$P_d = \langle I_d \rangle A_d \Omega_d \,, \tag{15}$$

where

$$\langle I_d \rangle = I_i \langle \text{BRDF}_d \rangle \cos\theta_i \, \Omega_i \,. \tag{16}$$

In Eq. (16), $I_i = P_s/A_s\Omega_s$ and $\langle BRDF_d \rangle$ is the mean value of the BRDF corresponding to the detector location and effective area,

$$\langle BRDF_d \rangle \equiv \frac{1}{M_d} \sum_{M_d} BRDF_{m_d} , \tag{17}$$

where M_d is the number of reflected rays collected by the detector. Recognizing that the apparatus has been fabricated so that $A_s\Omega_s = A_d\Omega_d = A\Omega$, we combine Eqs. (15) and (16) to obtain

$$\langle BRDF_d \rangle = \frac{P_d/P_s}{\Omega \cos\vartheta_i} = \frac{P_d/P_s}{(\pi r/R)^2 \cos\vartheta_i} . \tag{18}$$

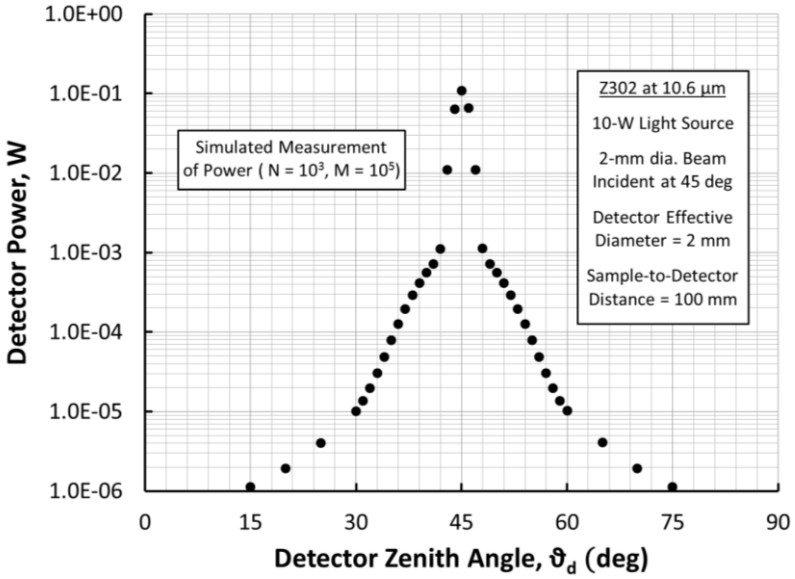

Fig. 10 Power measured by the detector using the apparatus of Fig. 9.

With the introduction of numerical values from the current example into Eq. (18), we have $\langle BRDF_d \rangle \cong 450\ P_d$. Thus, the peak value in Fig. 10, where $P_d = 0.109$ W, corresponds to a BRDF of 49 sr^{-1}, which is approximately one-half the "true" value calculated directly using the four-component model. This apparent discrepancy may be attributed to several factors, but it is mainly due to the finite size of the detector, whose angular extent is 1.145 deg, and to the local rate of change of BRDF with detector zenith angle near 45 deg. The apparatus measures the mean value of BRDF over the effective detector area. Therefore, results obtained near the reflection peak significantly underestimate the real BRDF values. Other factors contributing to the low value of "measured" BRDF are the finite size of the illuminating beam, whose diameter is 2.0 mm, and the limited distance from the coupon to the detector, 100 mm. The inherent inaccuracy of the numerical model itself (N = 1000 incident rays and M = 100,000 reflected rays) must also be considered, although this can be minimized by increasing N and M until the results obtained are no longer sensitive to their values. When the source and detector diameters are decreased from 2.0 to 1.0 mm and the number of rays traced is increased from N = 1000 to N = 10,000, the value obtained by the simulation for BRDF at $\varphi_d = 45$ deg increases from 49 to 81 sr^{-1}.

Modeling the apparatus using the MCRT method permits a parametric study to be carried out to determine the optimum values of P_s, r and R. For example, inspection of Fig. 10 reveals that if a single detector is to be used at all reflection angles, it must have a dynamic range covering six orders of magnitude and a sensitivity extending down into the low microwatt range. Furthermore, increasing the source power to obtain a higher detector power at large incidence angles might produce intolerably high heat fluxes on the coupon. Similarly, decreasing the radius r to increase the accuracy of the BRDF measurement near the peak also increases the local heat flux on the sample. The MCRT method is clearly a tremendously valuable tool for experimental design and optimization.

5. APPLICATION OF THE METHOD IN THE PRESENCE OF MULTIPLE REFLECTIONS

In the previous example rays reflected from the coupon were "lost"; that is they either were completely absorbed by the detector or by the surroundings. This greatly simplifies the process. We now briefly consider the MCRT method when use to calculate the power of bidirectionally reflected rays within enclosures consisting of multiple surfaces.

The following development is limited to implementation of continuation (2), described in the paragraph under Fig. 7, in which the power of the reflected ray is reduced with each reflection. For purposes of discussion let us assume that after three reflections the remaining ray power is below some predetermined threshold value, say one-tenth of a percent of the power of the original ray. This would probably be adequate for an enclosure whose surfaces were coated with Z302. We can easily extend the process to larger numbers of reflections by inductive reasoning.

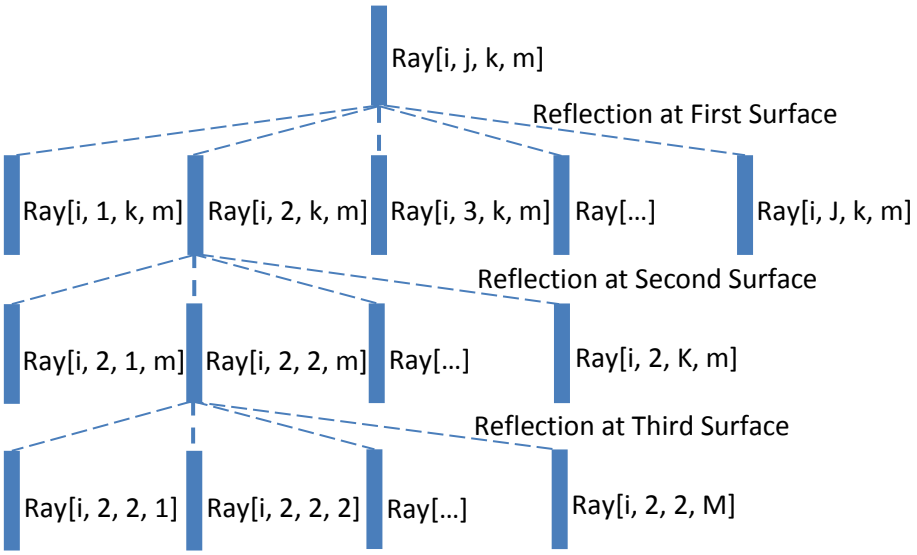

Fig. 11 Three-bounce life cycle of the i^{th} ray entering an enclosure made up of bidirectionally reflecting surfaces.

Referring to Fig. 11, in the case of three reflections, each ray has four indices (i, j, k, m). The index i indicates the i^{th} of I rays entering the enclosure. The i^{th} ray is reflected at a first bidirectional surface. This ray produces a maximum number of reflected rays, J, with each ray j carrying a power calculated from the BRDF model. Next, a ray which is reflected from the first surface will arrive at a second bidirectional surface. Upon reflection, this ray produces K rays with their indices k and power calculated from the BRDF model. We continue the MCRT method with a third bidirectional surface from which M rays are reflected carry the index m. The threshold method greatly reduces the computer workload, and so permits consideration of a large number of surfaces.

6. SUMMARY AND CONCLUSIONS

We demonstrate creation of a bidirectional reflectivity model based on BRDF data for Z302. We then give a brief example of using the model in the MCRT environment to simulate the very experiment used to obtain the original data. The example provides insight into the interplay between the optical model resolution and the number of rays that must be traced to obtain an accurate simulation, while also demonstrating the value of such a simulation in experimental design. Finally, in a brief coda we indicate the structure of the numerical algorithm required to treat multiple reflections within an enclosure composed of bidirectionally reflecting surfaces. We conclude from the brief example presented that the methodology elaborated in this contribution can produce accurate simulation of radiant exchange among the surfaces of such enclosures.

ACKNOWLEDGMENT

The effort reported in this contribution was sponsored by NASA's Langley Research Center in support of the Radiation Budget Instrument project.

REFERENCES

[1] Mahan, J. Robert, *Radiation Heat Transfer: A Statistical Approach*, New York: John Wiley & Sons, p. 84, (2002).
[2] A.Ono, "Calculation of the directional emissivities of cavities by the Monte Carlo method," *J. Opt. Soc. Am.*, 70(5), pp. 547–554, (1980).
[3] V. I. Sapritsky and A. V. Prokhorov, "Calculation of the effective emissivities of specular-diffuse cavities by the Monte Carlo method," *Metrologia*, 29(1), pp. 9–14, (1992).
[4] Y. Ohwada, Influence of deviation from Lambertian reflectance on the effective emissivity of a cavity, *Metrologia*, 32(6), pp. 713–716, (1996).
[5] A.V. Prokhorov, Monte Carlo method in optical radiometry, *Metrologia*, 35(4), pp. 465-471, (1998).
[6] Prokhorov, Alexander, and Nina I. Prokhorova, "Application of the three-component bidirectional reflectance distribution function model to Monte Carlo calculation of spectral effective emissivities of nonisothermal blackbody cavities," *Applied Optics*, 51(33), pp. 8003-8012, (2012).
[7] Anon, *Aerospace coatings: Z302 Absorptive Polyurethane – Black*, Retrieved August 8, 2017 from https://www.chembar.com/product/lord-aeroglaze-z302-absorptive-polyurethane-black/.